



## Strength-Adaptive Blast Design for Optimized Rock Fragmentation and Controlled Ground Vibrations



Nidumukkala Sri Chandras<sup>1\*</sup>, Yewuhalashet Fissha<sup>2</sup>, Nageswara Rao Cheepurupalli<sup>3</sup>

<sup>1</sup> Department of Mining Engineering, Malla Reddy Engineering College, 500014 Hyderabad, India

<sup>2</sup> Department of Geosciences, Geo-Technology and Materials Engineering for Resources, Graduate School of International Resource Sciences, Akita University, 010-8502 Akita, Japan

<sup>3</sup> Mining Engineering Department, Aksum University, 7080 Aksum, Ethiopia

\* Correspondence: Nidumukkala Sri Chandras (Srichandru2009@gmail.com)

Received: 03-16-2024

Revised: 05-08-2024

Accepted: 05-24-2024

**Citation:** N. S. Chandras, Y. Fissha, and N. R. Cheepurupalli, "Strength-adaptive blast design for optimized rock fragmentation and controlled ground vibrations," *GeoStruct. Innov.*, vol. 2, no. 2, pp. 102–115, 2024. <https://doi.org/10.56578/gsi020205>.



© 2024 by the author(s). Published by Acadlore Publishing Services Limited, Hong Kong. This article is available for free download and can be reused and cited, provided that the original published version is credited, under the CC BY 4.0 license.

**Abstract:** Achieving efficient fragmentation and minimizing ground vibration in blasting operations necessitates a precise understanding of bench geology, structural dimensions, and the compressive strength of the rock. This study presents a novel blast design approach that integrates compressive strength-driven adjustments to decking lengths and firing patterns, aiming to balance effective fragmentation with safe peak particle velocity (PPV) levels. A series of 36 trial blasts was conducted to assess the impact of decking and firing configurations tailored to specific rock strengths, supported by advanced software simulations and field laboratory testing. Results indicated that a combination of 3.5 m decking length with a V-pattern firing arrangement yielded optimal outcomes for rocks exhibiting compressive strengths between 40 and 50 MPa. This configuration achieved a mean fragmentation size (MFS) of 0.21 m and a PPV of 1.11 mm/s, demonstrating its suitability for controlled and efficient blasting. The findings underscore the critical role of rock strength in guiding blast design and provide mining engineers with practical insights for improving blast efficiency and safety. This study contributes to the development of adaptable blasting models that account for geological variability, paving the way for more precise control over fragmentation and ground vibration in complex mining environments.

**Keywords:** Fragmentation; Peak particle velocity; Decking length; Firing patterns; Blast design

### 1 Introduction

The use of chemical energy from explosives for rock breakage is highly economical compared to other mechanical methods of energy application. However, if it is not effectively utilized for fragmentation or material displacement, excessive ground vibration, fly rock, and noise can be caused. Desired fragmentation varies based on equipment size and type used at the mining face and throughout material handling processes. Efficient movement of blasted material, known as the muck profile, is essential for loading operations. Therefore, careful placement of boreholes relative to rock fractures and weak points and ensuring optimal burden spacing are crucial to maximize energy efficiency without unnecessary waste. One of the key aspects of blast optimization is tailoring fragmentation to meet the requirements of equipment used at the mining face and during material handling processes. Poorly fragmented material can lead to operational inefficiencies, including delays in loading and increased wear on equipment, which, in turn, results in higher operational costs [1]. For instance, mismatches between fragmentation and equipment capacity can cause bottlenecks in loading and hauling operations, while excessively fine fragmentation can overwhelm crushers, leading to higher energy consumption and downtime [2].

Moreover, the efficient displacement and movement of blasted material, referred to as the muck profile, are crucial for maintaining smooth loading operations. Proper borehole placement, relative to natural geological structures like fractures and weak planes, is essential to maximize the transfer of explosive energy into the rock mass, resulting in better fragmentation and reduced energy wastage [3]. Optimal burden and spacing configurations further contribute to achieving these outcomes by ensuring the energy is effectively utilized for fragmentation and displacement rather than wasted in generating excessive ground vibrations or fly rock [4].

The selection of proper decking length can significantly enhance fragmentation by ensuring better energy distribution in hard rock formations. Shorter decking lengths are known to improve fragmentation but may lead to higher PPV, whereas longer decking reduces vibrations but may result in coarser fragmentation [5]. Similarly, decking can also be used to reduce overbreak, control blast-induced vibrations, and improve energy distribution across the blasthole [6, 7]. Research indicates that V-shaped and staggered firing patterns enhance fragmentation by promoting progressive breakage and reducing stress concentrations, leading to uneven fragmentation and increased PPV. These firing patterns can effectively minimize backbreak and enhance rock fragmentation, while also controlling PPV compared to linear or parallel patterns [8, 9]. Moreover, V firing patterns in combination with optimal decking lengths have been found to produce finer fragmentation and lower PPV, particularly in hard rock formations. The inert material separating charges prevent simultaneous detonation of all charges, reducing the shockwave intensity and, therefore, the PPV [10]. However, improper decking (either too short or too long) can lead to uneven fragmentation and poor control over PPV.

The length and placement of decking play crucial roles in blast design and execution [11]. Decking involves dividing explosive charges into sections within blastholes using stemming [12]. While shorter blastholes with lower explosive consumption may not yield optimal results, longer decking lengths typically offer the best cost-effectiveness [13]. Increasing decking length not only enhances blast effectiveness but also optimizes cost efficiency by reducing the amount of explosive used [14]. Effective decking ensures more uniform distribution of explosive energy along the blasthole length, leading to improved fragmentation [15]. Maintaining decking lengths between 0.60 and 0.80 m has been found to achieve efficient rock breakage while minimizing the risk of sympathetic detonation. Optimal results, including lower ground vibration levels (PPV) of 1.22 mm/s, have been observed with a standardized decking length of 0.70 m [16], decking reduces the charge weight per delay without compromising vibration levels [17]. In recent trials, conventional solid decking with drill cuttings was employed to decrease PPV and achieve optimal fragmentation.

The blast pattern significantly influences both fragmentation results and ground vibration [18]. Firing patterns play a crucial role in determining burden and spacing, affecting secondary crushing once the rock mass is in motion. Under similar conditions, the V-pattern has been observed to produce finer fragmentation [19]. Research indicates that different blast patterns, such as the V, diagonal and line patterns, impact fragmentation by controlling the propagation of shock waves and the interaction of stress waves within the rock mass [20]. For instance, the V-pattern is noted for its ability to produce finer fragmentation due to its more effective distribution of energy across the blast area. This distribution enhances the uniformity of rock breakage, reducing the generation of oversized fragments and improving the efficiency of subsequent handling and processing operations [21].

In terms of ground vibration, blast patterns influence the propagation of seismic waves through the rock mass [22]. Patterns that distribute energy evenly help mitigate PPV and the air overpressure level, which are critical for minimizing environmental impact and ensuring compliance with regulatory limits [23, 24].

As the compressive strength of the rock mass increases, both MFS and PPV also increase in magnitude and intensity [25]. Rocks with higher compressive strength can be economically broken and fragmented because they can retain a larger proportion of the explosive energy. Higher rock compressive strength helps in minimizing the absorption of seismic waves and facilitates their transmission. Consequently, reduced attenuation in the wave transmission through the rock results in higher PPV [26, 27].

## 2 Methods and Materials

### 2.1 Field Data Collection

Data was collected from opencast mine I, Ramagundam region III area, SCCL, Telangana, India. The mine used to be underground, but it was converted to opencast. The overburden (OB) benches were 12 m high. The sandstone and alluvium soil that composed the rock strata were highly brittle. Sandstone was 2.3 g/cc in terms of density. Figure 1 depicts the site location and the experimental site.

### 2.2 Collection of Rock Core Samples and Uniaxial Compressive Strength (UCS) Testing

For the re-configuration of the new blast design, an AMIL single-core barrel machine was used to collect rock core samples, as shown in Figure 2, Figure 3, Figure 4. Figure 2 illustrates the AMIL S7802 single-core drilling machine used for onsite core sampling. The machine operated at 600 rpm with an NX-size diamond core bit (54 mm). Including the bit, the total weight of the device was 28 kg, powered by a 230 V, 10.5 A TMTL engine 70 KVA generator, as shown in Figure 3. To mitigate leveling and vibration issues, a bench was graded at the target site prior to assembly. The core barrel was internally greased for smooth sample extraction, secured with three surface bolts and one earth-anchor bolt for stability.

During coring, careful attention was paid to avoid uneven surfaces that could lead to sample breakage or jamming. Continuous water supply ensured optimal penetration into rock strata, while strict avoidance of manual anti-clockwise shaft rotation prevented core damage. Rock cores were extracted where in-situ stresses and rock mass discontinuities

were minimal, resulting in 11 cm long cores, conforming to the Indian Society of Rock Mechanics (ISRM) standards, as depicted in subgraph (a) of Figure 4 and subgraph (b) of Figure 4. A total of 40 core samples were obtained from four benches, collected both on the surface and at 10 m intervals along the cross-section from crest to toe. All samples were meticulously stored in a 2 ft core barrel case, shielded from moisture to maintain dry conditions.

Subsequently, the 40 rock specimens underwent sizing using a rock cutting machine, with both surface ends ground to ensure uniformity, as shown in subgraph (a) of Figure 5, subgraph (b) of Figure 5, and subgraph (c) of Figure 5. According to the ISRM standards, all samples maintained an Length-to-Diameter (L/D) ratio of 2 and a length of 10-12 cm. Each rock specimen was placed on the bottom plate of a compression machine, with the upper plate gradually lowered to make contact. Both the ring and dial gauge were zeroed prior to testing. Axial strain was applied at a rate of 2-12% per minute, with measurements taken every 30 seconds up to 6% strain. Dial gauge and proving ring readings were monitored every 60 seconds up to 12% strain. Testing continued until a maximum axial strain of 20% was reached or clear failure surfaces were observed.

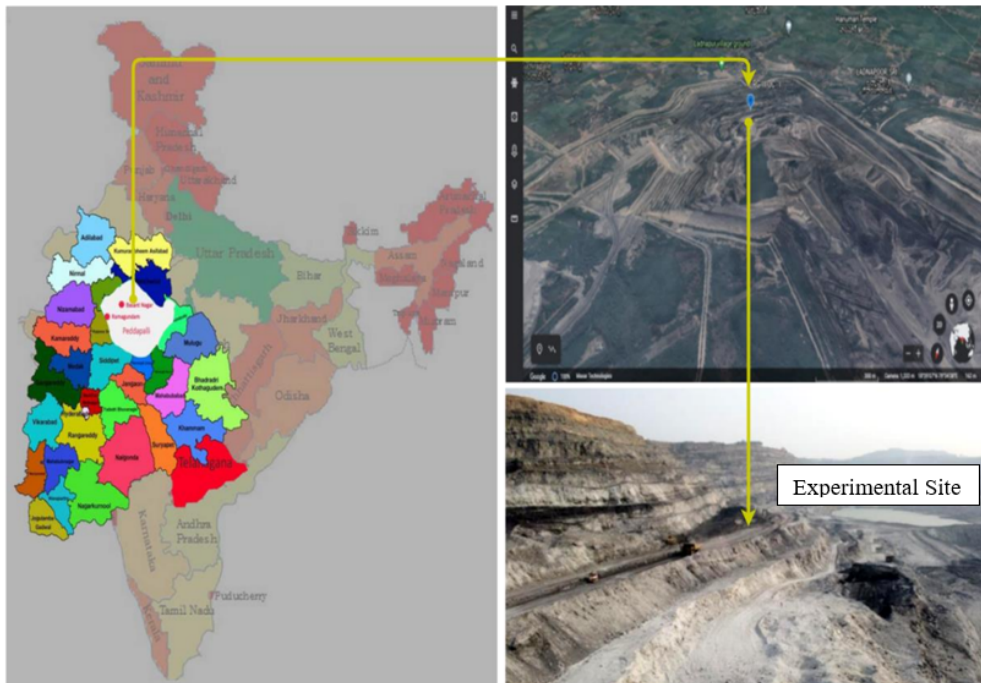


**Figure 1.** Location of the experiment site on the map of India



**Figure 2.** Coring machine



**Figure 3.** Generator



**Figure 4.** (a) Core sample; (b) Core barrel box with samples

### 2.3 Blast Modeling

#### 2.3.1 Blast design

All blasting operations were meticulously designed using O-PITBLAST software, incorporating RENISHAW 3D laser scanning technology to visualize blasts in a multi-dimensional format, thereby providing early warning insights, as illustrated in Figure 6. The design process integrates considerations of rock compressive strength to optimize blast efficacy.

Each blast was tailored with a focus on multi-decking, firing patterns, and adjusting the Stemming to Burden (Se/Be) ratio based on specific geological and spatial requirements. For instance, a typical design includes a 12 m bench utilizing SME explosives, featuring alternate decking lengths of 0.5 m, 2.5 m, and 1 m, fired in a V-pattern

configuration, as shown in Figure 7. This approach ensures that each blast achieves desired fragmentation outcomes while adhering to safety protocols and environmental considerations.

The User Interface (UI) has the ability to examine subtleties like a connection defect, overcharge, burden distribution, hole inclination, stemming, deck misplacement, and structural issues in the area of the blast, as illustrated in Figure 7.

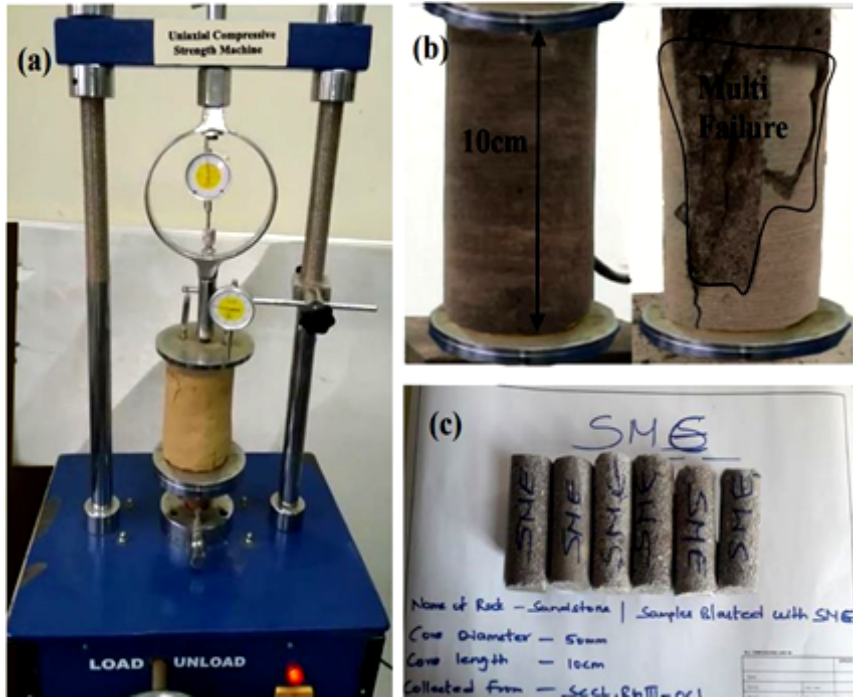


**Figure 5.** (a) UCS testing procedure; (b) Specimen failure; (c) Samples

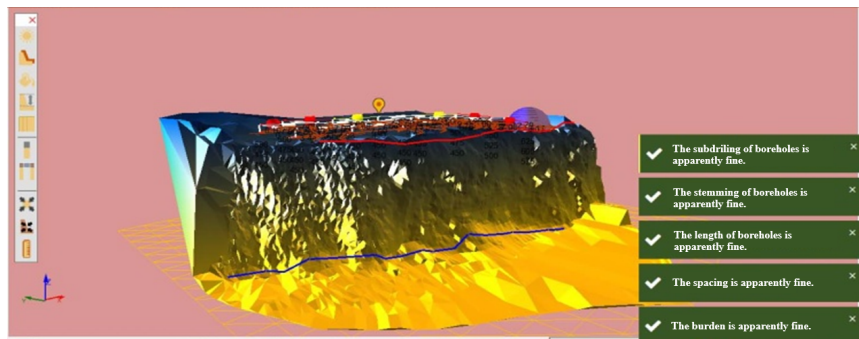


**Figure 6.** Blast design in software

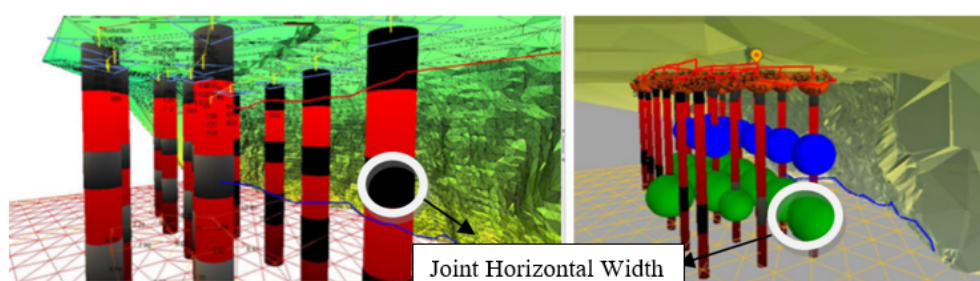


**Figure 7.** Multi-decking charging in software

### 2.3.2 Blast prediction

Predicted blast fragmentation for all blasts was based on a new set of blast parameters, with changes in blast geometry influencing predicted fragmentation sizes determined by software. The Kuznetsov concept was utilized for fragmentation prediction, categorizing sizes into X20, X50, X80, and X90, as depicted in Figure 8.

Figure 9 illustrates trends in PPV relative to scaled distances. Data on maximum charge per delay, distances measured, and monitored vibration parameters, such as PPV and peak vector sums in transverse and longitudinal directions, were analyzed. A least-squares regression model in logarithmic mode was employed to establish regression trends, determining optimal fit for blast vibration estimation with confidence levels of 50% and 95%. PPV values for each blast were predicted using a new attenuation law generated by O-PITBLAST, ensuring compliance with safety and environmental regulations.

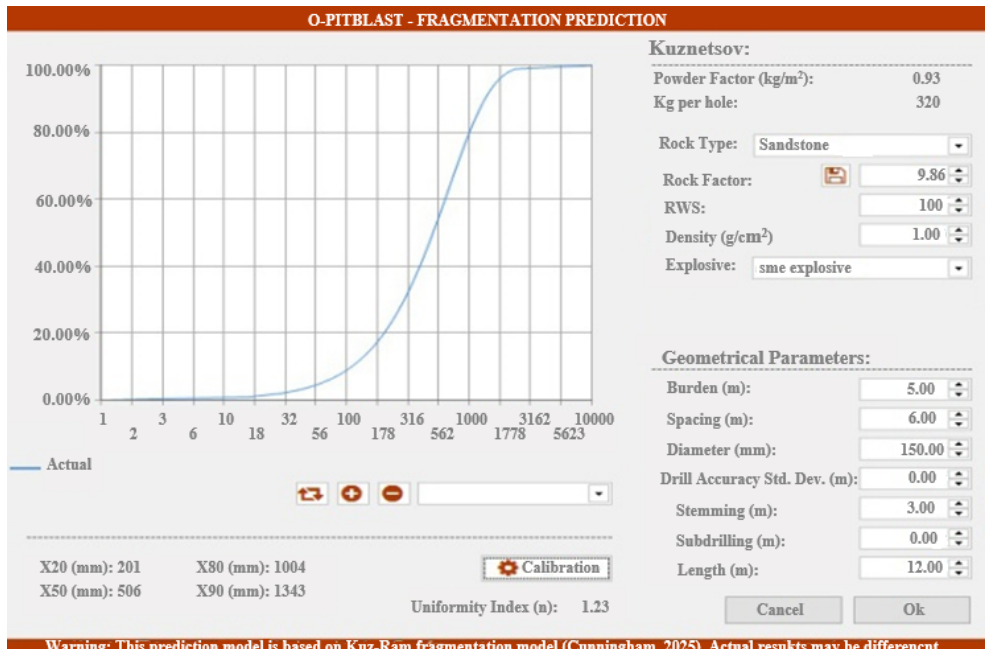


**Figure 8.** Fragmentation prediction

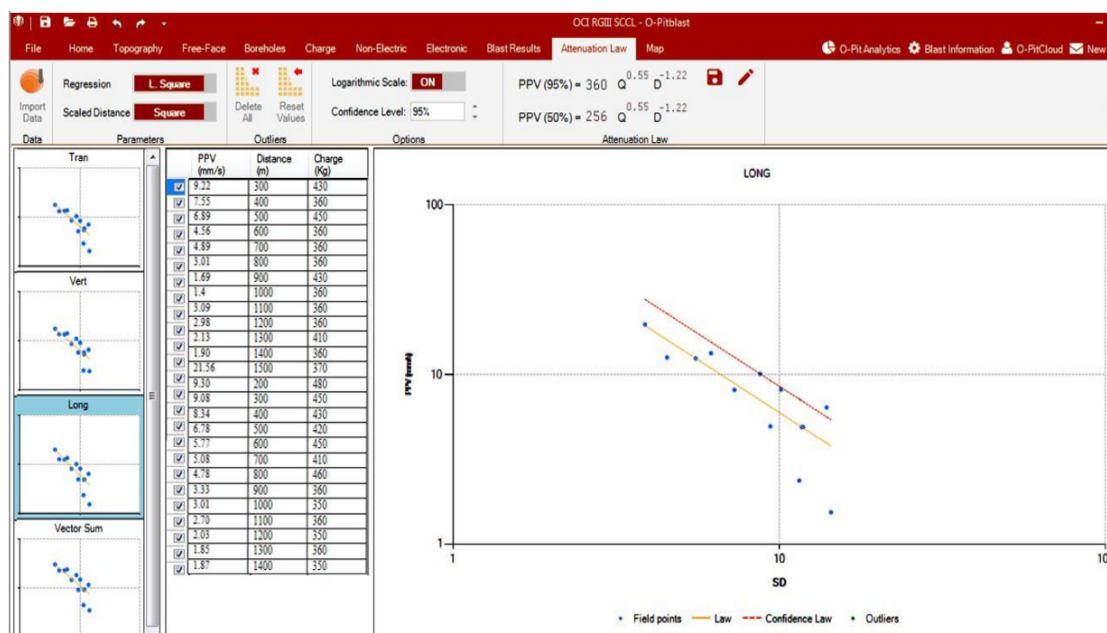


**Figure 9.** PPV prediction with attenuation law

### 3 Blast Experimentation

Three OB benches, each with a height of 12 m, were chosen for the study. The mine has historical underground operations, leading to concerns about strata disturbance and fracture generation. Designed burden and spacing values used in O-PITBLAST are detailed in Table 1, alongside accurately predicted outcomes. Figure 10, Figure 11 and Figure 12 illustrate the site location, experimental benches, firing patterns and charging composition.

Triple and double decking configurations were employed, taking into account the compressive strength of the adjacent rock, as detailed in Table 2. A total of 36 blasts were conducted to assess the influence of multiple decking and firing patterns on rock fragmentation and ground vibration based on rock compressive strength. SME was uniformly employed in all blasts, supplemented by booster explosives in conjunction with Non-Electric Detonators (NONEls). Delays of 475 and 450 ms were utilized according to the decking pattern. The average amount of explosives used ranged between 45 and 55 kg. Figure 9 illustrates the typical configuration of charging for these blasts. These blasts were conducted across three phases: A, B, and C, each involving 12 blasts on three separate benches.

**Table 1.** Key parameters of our model

| S/N | Bench Name | Phase   | Blast No. | No. of Rows | No. of Holes | Hole Diameter (mm) | Average Spacing Depth (m) | Front Hole (Se/Be) | Burden Ratio (m) | Front Burden (m) | No. of Decks | Deck Length (m) | Stemming Length (m) | Average Explosive per Hole (kg) | Total Explosive (kg) | Firing Pattern |
|-----|------------|---------|-----------|-------------|--------------|--------------------|---------------------------|--------------------|------------------|------------------|--------------|-----------------|---------------------|---------------------------------|----------------------|----------------|
| 1   |            |         | A1        | 3           | 27           | 150                | 12                        | 1.3                | 2.5              | 3                | 3            | 3               | 275                 | 7,425                           | Line                 |                |
| 2   |            | Phase A | A2        | 5           | 27           | 150                | 12                        | 1.2                | 2.5              | 2                | 3            | 3               | 375                 | 10,125                          | V                    |                |
| 3   | I          |         | A3        | 3           | 27           | 150                | 12                        | 1.3                | 2.5              | 2                | 3            | 3               | 300                 | 8,100                           | Diagonal             |                |
| 4   | De-coaled  |         | B1        | 3           | 27           | 150                | 12                        | 1.3                | 2.5              | 3                | 1.5          | 3               | 310                 | 8,230                           | V                    |                |
| 5   | seam       | Phase B | B2        | 3           | 27           | 150                | 12                        | 1.3                | 2.5              | 3                | 2.5          | 3               | 300                 | 8,100                           | V                    |                |
| 6   | bench      |         | B3        | 3           | 27           | 150                | 12                        | 1.3                | 2.5              | 3                | 3.5          | 3               | 300                 | 8,100                           | V                    |                |
| 7   |            |         | D1        | 3           | 27           | 150                | 12                        | 1.3                | 2.5              | 2                | 1.5          | 3               | 190                 | 5,130                           | Diagonal             |                |
| 8   |            | Phase C | D2        | 3           | 27           | 150                | 12                        | 1.3                | 2.5              | 2                | 2.5          | 3               | 290                 | 7,100                           | Diagonal             |                |
| 9   |            |         | D3        | 3           | 27           | 150                | 12                        | 1.3                | 2.5              | 2                | 3.5          | 3               | 220                 | 5,940                           | V                    |                |
| 10  |            |         | A4        | 3           | 27           | 150                | 10.5                      | 1.2                | 2.5              | 2                | 3            | 3               | 210                 | 6,110                           | Line                 |                |
| 11  |            | Phase A | A5        | 3           | 27           | 150                | 10.5                      | 1.3                | 2.5              | 2                | 3            | 3               | 270                 | 7,290                           | Diagonal             |                |
| 12  | 3A         |         | A6        | 3           | 27           | 150                | 10.5                      | 1.3                | 2.5              | 2                | 3            | 3               | 225                 | 4,500                           | V                    |                |
| 13  | De-coaled  |         | B4        | 3           | 27           | 150                | 10.5                      | 1.3                | 2.5              | 2                | 1.5          | 3               | 230                 | 6,210                           | V                    |                |
| 14  | seam       | Phase B | B5        | 3           | 27           | 150                | 10.5                      | 1.3                | 2.5              | 2                | 2.5          | 3               | 220                 | 5,940                           | V                    |                |
| 15  | bench      |         | B6        | 3           | 27           | 150                | 10.5                      | 1.3                | 2.5              | 1                | 3.5          | 3               | 245                 | 6,615                           | V                    |                |
| 16  |            |         | D4        | 3           | 28           | 150                | 10.5                      | 1.3                | 2.5              | 2                | 1.5          | 3               | 200                 | 5,400                           | Diagonal             |                |
| 17  |            | Phase C | D5        | 3           | 27           | 150                | 10.5                      | 1.3                | 2.5              | 2                | 2.5          | 3               | 185                 | 4,995                           | V                    |                |
| 18  |            |         | D6        | 3           | 27           | 150                | 10.5                      | 1.3                | 2.5              | 2                | 3.5          | 3               | 230                 | 6,210                           | Line                 |                |
| 19  |            |         | A7        | 3           | 27           | 150                | 11                        | 1.3                | 2.5              | 3                | 3            | 3               | 240                 | 6,480                           | V                    |                |
| 20  |            | Phase A | A8        | 3           | 29           | 150                | 11                        | 1.3                | 2.5              | 3                | 3            | 3               | 320                 | 9,280                           | Line                 |                |
| 21  |            |         | A9        | 3           | 27           | 150                | 11                        | 1.4                | 2.5              | 2                | 3            | 3               | 260                 | 7,020                           | Diagonal             |                |
| 22  | 3A         |         | B7        | 3           | 27           | 150                | 11                        | 1.2                | 2.5              | 2                | 1.5          | 3               | 250                 | 6,000                           | V                    |                |
| 23  | Seam       | Phase B | B8        | 3           | 28           | 150                | 11                        | 1.3                | 2.5              | 2                | 2.5          | 3               | 265                 | 7,420                           | V                    |                |
| 24  | bench      |         | B9        | 3           | 27           | 150                | 11                        | 1.2                | 2.5              | 2                | 3.5          | 3               | 270                 | 7,290                           | V                    |                |
| 25  |            |         | D7        | 3           | 27           | 150                | 11                        | 1.3                | 2.5              | 2                | 1.5          | 3               | 195                 | 5,265                           | V                    |                |
| 26  |            | Phase C | D8        | 3           | 27           | 150                | 11                        | 1.3                | 2.5              | 3                | 2.5          | 3               | 175                 | 4,725                           | Diagonal             |                |
| 27  |            |         | D9        | 3           | 27           | 150                | 11                        | 1.3                | 2.5              | 2                | 3.5          | 3               | 210                 | 5,670                           | V                    |                |

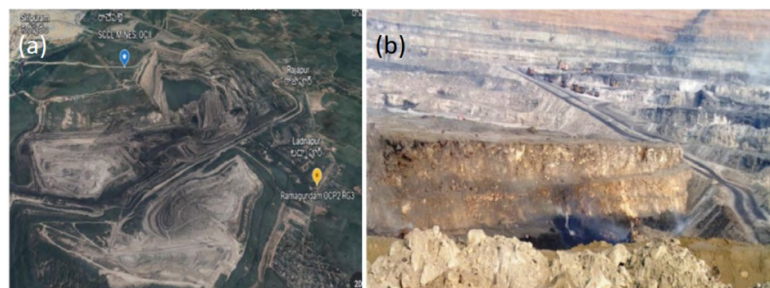


**Figure 10.** Location of the experiment site and experimental benches of SCCL Ramagundam mines

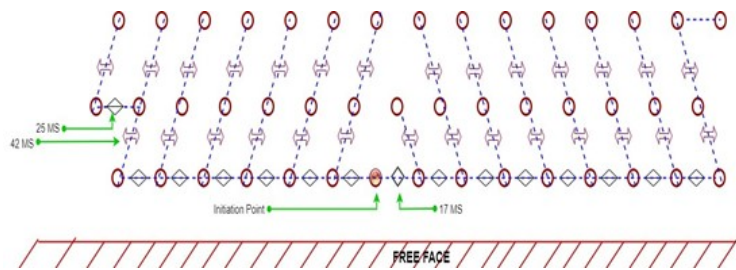


**Figure 11.** Systematic design of the V firing pattern adopted during experimentation

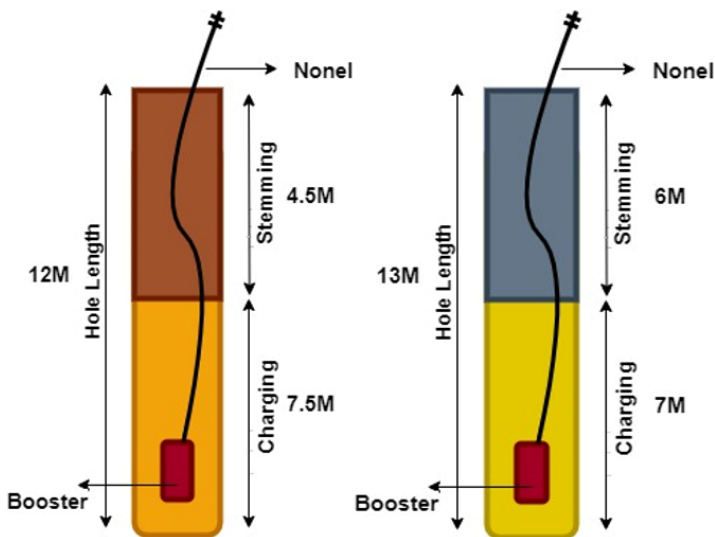


**Figure 12.** Explosive column charging for benches

**Table 2.** Blast results

| S.N | Blast No.               | Phase   | Fragmentation       |                 |                     |                 | Ground Vibration               |                   | Rock Compressive Strength (Mpa) |
|-----|-------------------------|---------|---------------------|-----------------|---------------------|-----------------|--------------------------------|-------------------|---------------------------------|
|     |                         |         | Prediction K50 (mm) | Actual K80 (mm) | Prediction D50 (mm) | Actual D80 (mm) | Distance Prediction PPV (mm/s) | Actual PPV (mm/s) |                                 |
| 1   | I De-coaled seam bench  | Phase A | 0.67                | 1.66            | 0.55                | 1.59            | 500                            | 4.91              | 4.33                            |
| 2   |                         |         | 1.4                 | 1.97            | 1.18                | 1.69            | 500                            | 4.26              | 3.29                            |
| 3   |                         |         | 0.91                | 1.43            | 1.2                 | 1.56            | 500                            | 4.78              | 2.94                            |
| 4   |                         |         | 1.2                 | 1.66            | 1.6                 | 2.49            | 500                            | 4.02              | 4.56                            |
| 5   |                         | Phase B | 0.89                | 1.34            | 0.78                | 1.16            | 500                            | 5.90              | 5.15                            |
| 6   |                         |         | 0.55                | 1.22            | 0.65                | 1.42            | 500                            | 4.22              | 4.79                            |
| 10  |                         |         | 0.44                | 0.89            | 0.65                | 2.08            | 500                            | 2.11              | 3.21                            |
| 11  |                         | Phase C | 0.38                | 0.97            | 0.89                | 1.13            | 500                            | 2.95              | 2.80                            |
| 12  |                         |         | 0.31                | 0.88            | 1.21                | 0.94            | 500                            | 2.04              | 2.21                            |
| 13  |                         | Phase A | 0.88                | 1.66            | 1.02                | 1.95            | 500                            | 3.20              | 3.52                            |
| 14  |                         |         | 1.1                 | 1.97            | 1.59                | 2.34            | 500                            | 3.01              | 2.78                            |
| 15  |                         |         | 0.91                | 1.43            | 0.89                | 1.22            | 500                            | 3.08              | 1.94                            |
| 16  |                         |         | 1.2                 | 1.66            | 0.911               | 1.39            | 500                            | 3.01              | 3.96                            |
| 17  | 3A De-coaled seam bench | Phase B | 0.82                | 1.44            | 0.89                | 1.82            | 500                            | 3.99              | 4.51                            |
| 18  |                         |         | 0.47                | 1.11            | 0.74                | 1.93            | 500                            | 2.21              | 3.55                            |
| 22  |                         |         | 0.38                | 0.75            | 1.3                 | 0.95            | 500                            | 2.04              | 2.55                            |
| 23  |                         | Phase C | 0.38                | 0.89            | 0.911               | 1.07            | 500                            | 1.94              | 2.03                            |
| 24  |                         |         | 0.34                | 0.79            | 0.6                 | 0.97            | 500                            | 2.21              | 2.85                            |
| 25  |                         |         | 0.57                | 1.83            | 0.88                | 1.73            | 500                            | 3.95              | 3.11                            |
| 26  | 3A Seam bench           | Phase A | 0.56                | 1.39            | 0.82                | 1.33            | 500                            | 3.23              | 2.09                            |
| 27  |                         |         | 0.91                | 1.43            | 1.6                 | 2.07            | 500                            | 3.91              | 1.11                            |

Phase A: The firing pattern was initially changed, and all other blast design parameters remained the same.

Phase B: All blast design parameters were kept constant and decking length and position were changed as per rock compressive strength.

Phase C: Decking length and firing patterns were changed together, as well as the consideration of the rock compressive strength, while the rest of the parameters remained unchanged.

## 4 Blast Result Analysis

### 4.1 Fragmentation Analysis and Ground Vibration Measurement

Ortho-photographs, photographs taken perpendicular to the field plane, were used to create a 3D fragmentation model based on point cloud data. These models utilized a digital terrain model to enhance a visual analysis of fragmentation within each muck pile corner. Percentages representing total rock with specific diameters or less were designated as D10, D20...D80, D90. These values were automatically generated based on the principles of the Kuznetsov-Rammler (Kuz-Ram) and Swedish Blasting Research Centre (SWEBREC) algorithms. Artificial intelligence (AI) technology was employed to assign different colors to various rock fragmentation sizes, as illustrated in Figure 13. Fragmentation graphs were generated for all blasts, and resulting color-coded plates were produced with AI assistance to visualize and analyze fragmentation outcomes accurately.

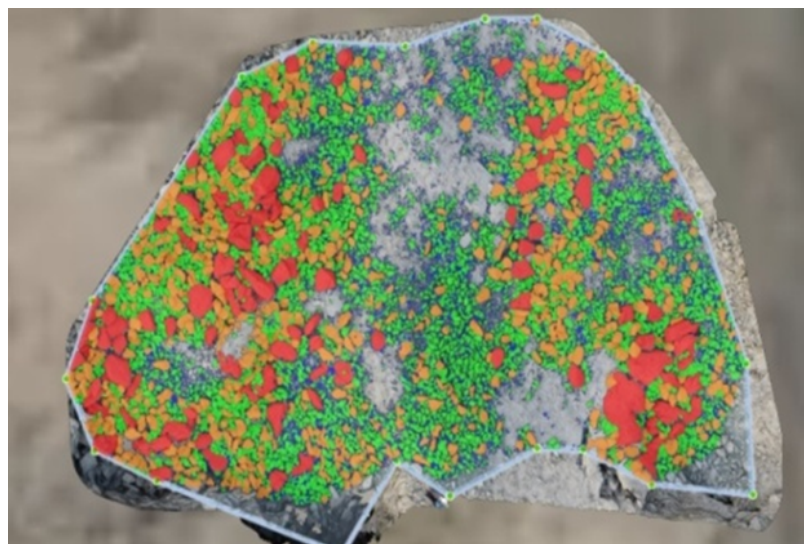


**Figure 13.** Muckpile detection

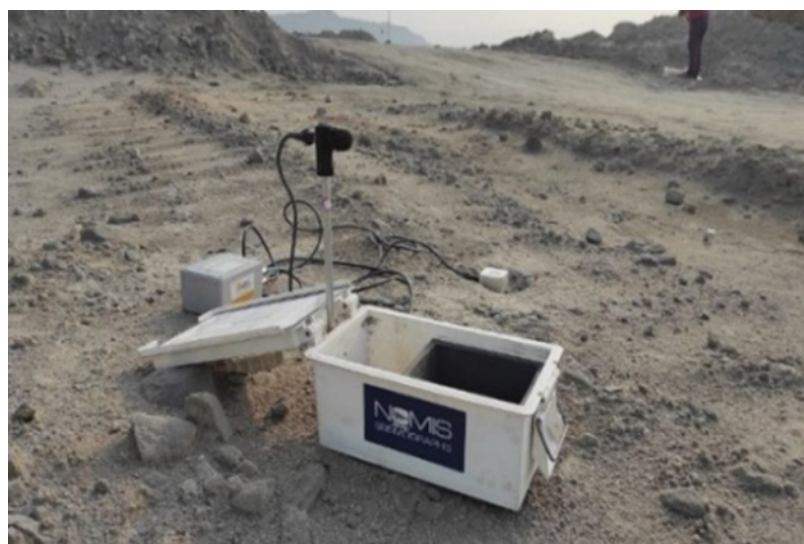


**Figure 14.** NOMIS seismograph at point

## 4.2 Ground Vibration Measurement

The NOMIS engineering seismograph, as depicted in Figure 14, was utilized to measure ground vibrations. The transducer, equipped with a sensor, was affixed to spikes securely driven into the ground to maintain contact with the earth's crust. The instrument was positioned at a distance of 500 m, measured using the drone technology. Ground vibration measurements were conducted for all 36 blasts. Each blast utilized a maximum charge delay ranging between 280-350 kg per hole. Vibration data for longitudinal (R), vertical (V), and transverse (T) components, as well as vector sum velocity (VS), were recorded by the seismograph during the blasts, as detailed in Table 2.

## 5 Discussions

### 5.1 Relationship Between Decking Length, MFS and PPV (Phase I)

In Phase I, decking lengths of 1.5 m, 2.5 m, and 3.5 m were utilized to optimize explosive usage where lower rock compressive strength was observed in the bench section. The selection of decking length was tailored based on the compressive strength of the rock at each site to investigate their impact on MFS and PPV. Incremental decking lengths were chosen considering the compressive strength of the rock columns. Due to pre-existing discontinuities that can reduce rock strength, less explosive was sufficient for effective fragmentation with precise placement. The minimum MFS observed over the three investigative benches was 0.73 m with a 1.5 m decking length, 0.82 m with a 2.5 m decking length, and 0.43 m with a 3.5 m decking length, as illustrated in subgraph (a) of Figure 15. Consequently, PPV was reduced due to effective sealing of cracks by the stemming. The graph indicates a decreasing trend in PPV, registering 1.11 mm/s with a 3.5 m decking length for boreholes, attributed to effective closure of joints and reduced transmission influenced by pre-existing discontinuities, as shown in subgraph (b) of Figure 15.

### 5.2 Relationship Between Firing Patterns, MFS and PPV (Phase II)

In Phase II, observations indicated that across all three firing patterns, the V pattern consistently produced favourable fragmentation sizes ranging from 0.35 to 0.41 m. The perpendicular firing initiation with the V pattern involved reducing hole burdens and increasing spacing at the initiation and during the collision of broken rock in flight, resulting in the lowest MFS of 0.41 m, as depicted in subgraph (a) of Figure 16.

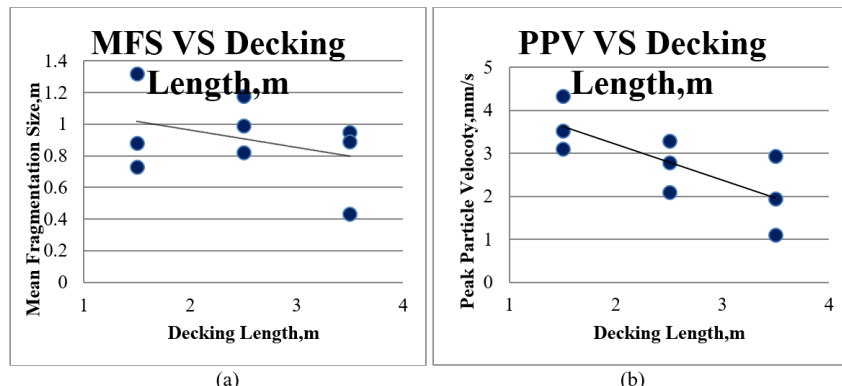


Figure 15. Relationship between decking length, MFS and PPV

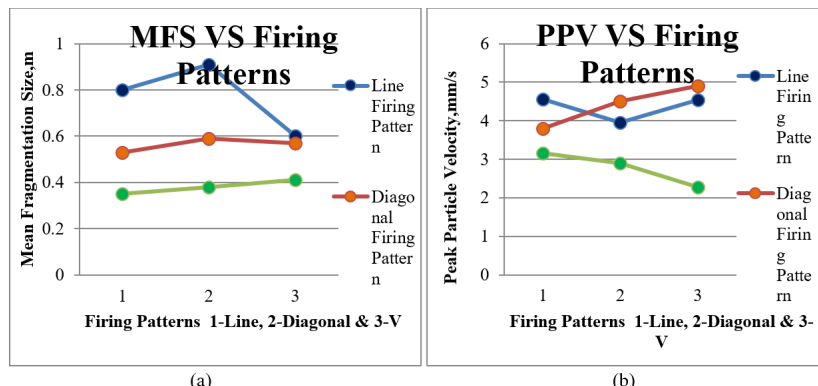


Figure 16. Relationship between firing patterns, MFS and PPV

Regarding PPV, safe levels ranging from 2.28 to 3.1 mm/s were consistently achieved at various monitoring distances with the V firing pattern. This outcome can be attributed to the cancellation of wave patterns generated by simultaneous holes on both arms of the V, contrasting with diagonal or line firing patterns. However, a few blasts recorded slightly higher PPV due to the presence of only one joint set, which did not attenuate vibrations but rather absorbed them. The lowest PPV recorded was 2.28 mm/s, as illustrated in subgraph (b) of Figure 16.

### 5.3 Relationship Between the Combination of Firing Patterns and Decking Lengths, MFS and PPV (Phase III)

Phase III sequentially explored the combined effects of decking length and firing pattern adjustments to optimize blast configurations based on the rock compressive strength. Decking lengths of 1.5 m, 2.5 m, and 3.5 m, along with firing patterns diagonal and V, were revisited due to their superior performance observed in previous phases.

Subgraph (a) of Figure 17 illustrates the relationship between MFS, decking length, and firing pattern. Decking was strategically placed to block primary horizontal seams, aligning with the specified decking lengths wherever feasible. The V firing pattern, coupled with a 3.5 m decking length, achieved an excellent MFS of 0.35 m. This approach reduced the amount of explosives used while intensifying their effectiveness in rocks with lower compressive strengths ranging from 35 to 41 MPa.

The lower PPV values indicate effective mitigation of geological discontinuities encountered in boreholes. A decking length of 3.5 m resulted in a significant reduction in PPV, registering 1.49 mm/s at 500 m, as shown in subgraph (b) of Figure 17, with a maximum of 2.85 mm/s observed at the same distance.

The MFS increased with higher compressive strength of the rock mass. When the rock strength ranged between 35 and 50 MPa, it consistently produced good fragmentation sizes of 0.35 to 0.65 m, with MFS showing a continuous rise with increasing UCS of the rock, as depicted in subgraph (a) of Figure 18.

Higher UCS indicates stronger rock components or more resilient cementing substances binding them together. Consequently, PPV tended to increase as rocks with higher UCS withstood greater detonation velocities before yielding to explosive forces. PPV escalated with UCS, facilitated by competent rock structures, allowing PPV to propagate through successive layers, as illustrated in subgraph (b) of Figure 18. For instance, at a rock UCS of 40 MPa, PPV was measured at 1.11 mm/s, demonstrating this trend. The varying compressive strength of the rock facilitated the selection of diverse blast combinations across all phases of the study.

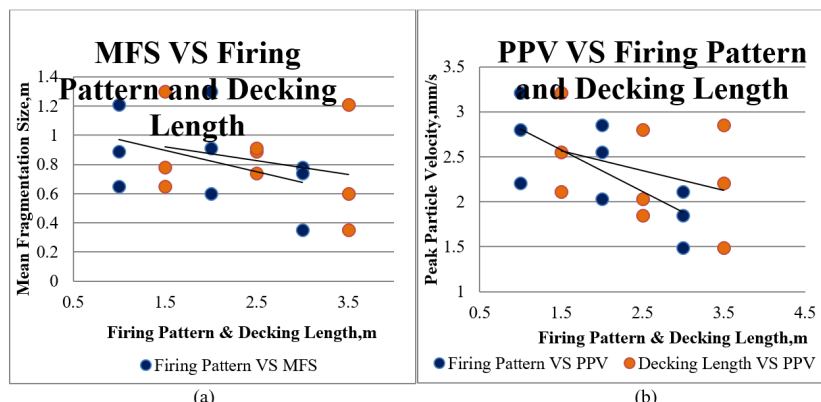


**Figure 17.** Relationship between the combination of firing patterns and decking lengths, MFS and PPV

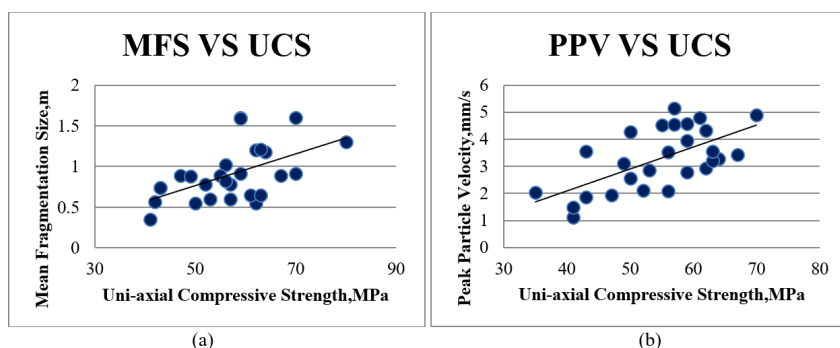


**Figure 18.** Relationship between UCS, MFS and PPV

## 6 Conclusion

- Drones significantly facilitated capturing blast fragmentation images in challenging environments where conventional methods are impractical. Their satellite-guided remote control simplifies determining directions and distances between desired sites.
- AI-based software excelled in accurately predicting and analyzing rock fragmentation sizes and ground vibrations with precision. The accuracy of these predictions is contingent upon the quality and quantity of drone-captured images.
- Optimal fragmentation and safe PPV were achieved by integrating re-engineered decking lengths and firing patterns with consideration of rock compressive strength, rather than treating them in isolation. For instance, a combination of 3.5 m decking length and V firing pattern produced a MFS of 0.21 m and a PPV of 1.11 mm/s.
- Rock with compressive strength between 40 and 50 MPa exhibited good fragmentation, although PPV increased with higher rock strength. Nevertheless, PPV values remained relatively low compared to phases A, B, and C.
- It was concluded in this study that by integrating decking length, firing pattern, and rock compressive strength considerations, blasting operations in OB benches can be conducted effectively and safely.

## 7 Limitations

The study's findings regarding optimal decking lengths and firing patterns were based on specific rock types and compressive strength ranges (40-50 MPa). While drones effectively captured blast fragmentation images in challenging environments, certain extreme weather conditions (e.g., heavy rain and fog) may hinder drone operations and image quality, potentially impacting the data's reliability. In addition, the accuracy of AI-based predictions regarding rock fragmentation sizes and ground vibrations relies heavily on the quality and quantity of drone-captured images. PPV values were found to be relatively low in the studied conditions; the inherent variability in rock properties and blast conditions could lead to differing results in practice, requiring careful consideration during implementation.

## 8 Future Work

Advanced image processing and machine learning techniques could be investigated and implemented to further improve the analysis of fragmentation images, potentially leading to better prediction outcomes. Field tests in diverse environmental and geological conditions could be conducted to help validate the findings regarding optimal decking lengths and firing patterns, enhancing their generalizability across different sites. In addition, the integration of drone technology with other monitoring systems (e.g., ground vibration sensors) could be explored, thereby providing a more comprehensive understanding of the interaction between blasting operations and their environmental impact. AI models could be refined by incorporating real-time data from ongoing blasting operations, improving predictive capabilities and facilitating more dynamic decision-making in blast design.

## Data Availability

The data supporting the findings of this study are available from the corresponding author upon reasonable request.

## Acknowledgements

I would like to express my heartfelt gratitude to my mentor, B.S. Choudhary, Associate Professor, IIT (ISM) Dhanbad, for meticulously tracking and adding his research inputs to this paper. I am always grateful to my college IIT (ISM) Dhanbad. I would like to express my gratitude to the Principal, Director, and management of Malla Reddy Engineering College, Hyderabad for allocating adequate time to carry out research.

## Conflicts of Interest

The authors declare no conflict of interest.

## References

- [1] A. Gebretsadik, R. Kumar, Y. Fissha, Y. Kide, N. Okada, H. Ikeda, A. K. Mishra, D. J. Armaghani, Y. Ohtomo, and Y. Kawamura, "Enhancing rock fragmentation assessment in mine blasting through machine learning algorithms: A practical approach," *Discov. Appl. Sci.*, vol. 6, p. 223, 2024. <https://doi.org/10.1007/s42452-024-05888-0>
- [2] Z. Zhang, J. Sanchidrián, F. Ouchterlony, and S. Luukkanen, "Reduction of fragment size from mining to mineral processing: A review," *Rock Mech. Rock Eng.*, vol. 56, pp. 747–778, 2023. <https://doi.org/10.1007/s00603-022-03068-3>

- [3] T. Bamford, F. Medinac, and K. Esmaeili, “Continuous monitoring and improvement of the blasting process in open pit mines using unmanned aerial vehicle techniques,” *Remote Sens.*, vol. 12, p. 2801, 2020. <https://doi.org/10.3390/rs12172801>
- [4] S. Prasad, B. Choudhary, and A. Mishra, “Effect of stemming to burden ratio and powder factor on blast induced rock fragmentation—A case study,” *IOP Conf. Ser. Mater. Sci. Eng.*, vol. 225, no. 012191, 2017. <https://doi.org/10.1088/1757-899X/225/1/012191>
- [5] J. Jhanwar, A. Chakraborty, V. Murthy, G. Saini, J. Jethwa, and B. Dhar, “Application of air-deck blasting technique to improve fragmentation and blast economics in the foot wall side of Dongri-Buzury open cast mine,” Central Mining Research Institute (CMRI), Unpublished CMRI Project Report MT/Collab/N/3/95, 1996.
- [6] F. Mohamed, B. Riadh, S. Abderazzak, N. Radouane, S. Mohamed, and T. Ibsa, “Distribution analysis of rock fragments size based on the digital image processing and the Kuz-Ram model: Case of Jebel Medjounes quarry,” *Ann. Min. Min. Sci.*, vol. 2, 2019. <https://doi.org/10.31031/AMMS.2019.02.000545>
- [7] P. K. Singh, M. P. Roy, R. K. Paswan, M. Sarim, S. Kumar, and R. Jha, “Rock fragmentation control in opencast blasting,” *J. Rock Mech. Geotech.*, vol. 8, no. 2, pp. 225–237, 2016. <https://doi.org/10.1016/j.jrmge.2015.10.005>
- [8] F. Faramarzi, H. Mansouri, and M. A. Ebrahimi Farsangi, “A rock engineering systems based model to predict rock fragmentation by blasting,” *Int. J. Rock Mech. Min. Sci.*, vol. 60, pp. 82–94, 2013. <https://doi.org/10.1016/j.ijrmms.2012.12.045>
- [9] K. Chakraborty, A. K. Raina, M. Ramulu, P. B. Choudhury, A. Haldar, P. Sahu, and C. Bandopadhyay, “Parametric study to develop guidelines for blast fragmentation improvement in jointed and massive formations,” *Eng. Geol.*, vol. 73, pp. 105–116, 2004. <https://doi.org/10.1016/j.enggeo.2003.12.003>
- [10] E. Hamdi and J. du Mouza, “A methodology for rock mass characterisation and classification to improve blast results,” *Int. J. Rock Mech. Min. Sci.*, vol. 42, no. 2, pp. 177–194, 2005. <https://doi.org/10.1016/j.ijrmms.2004.07.005>
- [11] J. C. Jhanwar, A. K. Cakraborty, H. R. Anireddy, and J. L. Jethwa, “Application of air decks in production blasting to improve fragmentation and economics of an open pit mine,” *Geotech. Geol. Eng.*, vol. 17, pp. 37–57, 1999.
- [12] A. K. Verma and T. N. Singh, “A neuro-fuzzy approach for prediction of longitudinal wave velocity,” *Neural Comput. Appl.*, vol. 22, no. 7-8, pp. 1685–1693, 2012. <https://doi.org/10.1007/s00521-012-0817-5>
- [13] M. Hasanipanah, D. Jahed Armaghani, H. Bakhshandeh Amniah, M. Z. A. Majid, and M. M. D. Tahir, “Application of PSO to develop a powerful equation for prediction of flyrock due to blasting,” *Neural Comput. Appl.*, vol. 28, no. S1, pp. 1043–1050, 2016. <https://doi.org/10.1007/s00521-016-2434-1>
- [14] V. M. Kuznetsov, “The mean diameter of the fragments formed by blasting rock,” *Sov. Min. Sci.*, vol. 9, pp. 144–148, 1973.
- [15] A. Nourian and H. Moomivand, “Development of a new model to predict uniformity index of fragment size distribution based on the blasthole parameters and blastability index,” *J. Min. Sci.*, vol. 56, pp. 47–58, 2020.
- [16] M. Hayat, L. Alagha, and D. Ali, “Air decks in surface blasting operations,” *J. Min. Sci.*, vol. 55, no. 6, pp. 922–929, 2019.
- [17] X. J. Zhang, X. G. Wang, Y. L. Yu, and D. Q. Yang, “The application of deck charge technology in Hua Neng open pit mine,” *E3S Web of Conf.*, vol. 38, p. 03031, 2018. <https://doi.org/10.1051/e3sconf/20183803031>
- [18] M. Hasanipanah, R. Naderi, J. Kashir, S. A. A. Noorani, and A. Z. Qaleh, “Prediction of blast-produced ground vibration using particle swarm optimization,” *Eng. Comput.*, vol. 33, no. 2, pp. 173–179, 2016. <https://doi.org/10.1007/s00366-016-0462-1>
- [19] P. Balamadeswaran, A. K. Mishra, P. Sen, and S. Ramesh, “Investigations into the influence of decking on rock fragmentation and ground vibrations by blasting in shallow benches of limestone quarries—a case study,” *J. Mines Met. Fuels*, vol. 66, 2018. <https://doi.org/10.18311/jmmf/2018/27974>
- [20] B. Gordani, D. Jahed Armaghani, M. Hajihassani, and M. Monjezi, “Prediction of seismic slope stability through combination of particle swarm optimization and neural network,” *Eng. Comput.*, vol. 32, no. 1, pp. 85–97, 2015. <https://doi.org/10.1007/s00366-015-0400-7>
- [21] F. Chiappetta, “New blasting technique to eliminate subgrade drilling improve fragmentation reduce explosive consumption and lower ground vibrations,” *J. Explosives Eng.*, vol. 21, no. 1, pp. 10–12, 2004.
- [22] T. Sasaoka, Y. Takahashi, A. Hamanaka, S. Wahyudi, and H. Shimada, “Effect of delay time and firing patterns on the size of fragmented rocks by bench blasting,” *Springer Nat. Switz.*, pp. 449–456, 2019. [https://doi.org/10.1007/978-3-030-33954-8\\_51](https://doi.org/10.1007/978-3-030-33954-8_51)
- [23] N. S. Chandrasas, B. S. Choudhary, V. M. Teja, M. S. Venkatramayya, and N. S. R. Krishna Prasad, “XGBoost algorithm to simultaneous prediction of rock fragmentation and induced ground vibration using unique blast data,” *Appl. Sci.*, vol. 12, p. 5629, 2022.

- [24] T. Pradeep, N. S. Chandrahas, and Y. Fissha, “A principal component-enhanced neural network framework for forecasting blast-induced ground vibrations,” *J. Civ. Hydraul. Eng.*, vol. 2, no. 4, pp. 206–219, 2024. <https://doi.org/10.56578/jche020402>
- [25] N. S. Chandrahas, B. S. Choudhary, M. S. Venkataramayya, and F. Yewuhalashet, “An inventive approach for simultaneous prediction of mean fragmentation size and peak particle velocity using futuristic datasets through improved techniques of genetic XG boost algorithm,” *Min. Metall. Explor.*, vol. 41, pp. 2391–2405, 2024. <https://doi.org/10.1007/s42461-024-01045-8>
- [26] S. Chandrahas, B. S. Choudhary, M. Venkataramayya, F. Yewuhalashet, and B. O. Taiwo, “An investigation of the cumulative impact of decking length and firing pattern on blasting results,” *J. Min. Environ.*, 2024. <https://doi.org/10.22044/jme.2024.14555.2743>
- [27] N. S. Chandrahas, B. S. Choudhary, M. S. Venkataramayya, Y. Fissha, and N. R. Cheepurupalli, “AI-driven analysis of rock fragmentation: The influence of explosive charge quantity,” *Acadlore Trans. Geosci.*, vol. 3, no. 3, pp. 123–134, 2024. <https://doi.org/10.56578/atg030301>